

Ionogels in Aqueous Media: From Conductometric Probing of the Ionic Liquid Washout to the Design of More Stable Materials

Sergei Yu. Kottsov ¹, Alexandra O. Badulina ¹, Vladimir K. Ivanov ^{1,2}, Alexander E. Baranchikov ^{1,*}, Aleksey V. Nelyubin ¹, Nikolay P. Simonenko ¹, Nikita A. Selivanov ¹, Marina E. Nikiforova ¹ and Aslan Yu. Tsivadze ³

¹ Kurnakov Institute of General and Inorganic Chemistry of the Russian Academy of Science, Leninsky Prospekt, 31, 119991 Moscow, Russia

² Faculty of Materials Science, Lomonosov Moscow State University, Leninskiye Gory, 1, Building 73, 119991 Moscow, Russia

³ Frumkin Institute of Physical Chemistry and Electrochemistry of the Russian Academy of Science, Leninsky Prospekt, 31 k.4, 119071, Moscow, Russia

* Correspondence: a.baranchikov@yandex.ru

Table S1. Some properties of the ionic liquids used for the experiments *.

Ionic Liquid	BMIm DCA	EMIm TFSI	BMIm TFSI	OMIm TFSI
Molar weight, g·mol ⁻¹	205.26	391.31	419.36	475.47
Density, g·cm ⁻³	1.06	1.52	1.44	1.32
Conductivity, mS·cm ⁻¹	9.53	6.63	3.41	1.0
Electrochemical window, V	3.7 [1]	4.7	4.6	2.5 [2]
Viscosity, cP at 20°C	28	39.4	48.8	106
Melting point, °C	-6	-17	-4	-43
Hydrophilic/Hydrophobic [3]	Hydrophilic	Hydrophobic	Hydrophobic	Hydrophobic
Water solubility at 25°C, wt.%	Intermixable [4]	2.1	0.7 [4]	0.21 [4]

* Unless otherwise specified, the data was provided by the manufacturer in the corresponding specification.

Analysis of Ionogels

The apparent (geometric) density (ρ_{app}) of the samples was calculated from their weight, determined using an analytical balance ($\delta = 10^{-4}$ g), and geometric size, determined using digital calipers ($\delta = 0.02$ mm). The skeletal density of the samples (ρ_{sk}) was measured using a ThermoFisher Scientific Pycnomatic ATC helium pycnometer at 20°C. The volumetric porosity (P) of the ionogels was calculated as $P(\%) = 100\% \times (1 - \frac{\rho_{app}}{\rho_{sk}})$. The density of bare ionic liquids was also determined, using the same method (see Table 3 in the manuscript). For the measurements, 1.0 g aliquots were used.

The water contact angle on ionogel surfaces was measured using a Minder Hightech SDC-350 instrument with 0° stage inclination. The water droplet volume was ~5 μ L and the droplet shape was approximated using a 5-point ellipsoid model.

Low-temperature nitrogen adsorption experiments were conducted using a Katakion Sorbtometer-M low temperature nitrogen adsorption system. Prior to analysis, the samples were degassed in a dry helium flow at 120°C for 2 h. For the specific surface area (S_{BET}) calculation, five experimental points were measured in the partial pressure range of 0.05–0.25 P/P_0 and the Brunauer-Emmett-Teller (BET) model was applied after data validation using the Rouquerol criteria [5,6]. Full nitrogen adsorption-desorption isotherms were measured using the same system, in a P/P_0 range of 0.01–0.97. Pore size distribution was constructed within the Barrett-Joyner-Halenda (BJH) model, using the desorption branch of the isotherm. To assess the volume of micropores in the samples, Dubinin-

Radushkevich (DR) model-based estimations were made. The PyGAPS software package was used to process the experimental data [7].

X-ray diffraction (XRD) patterns were collected on a Haoyuan DX-200BH powder diffractometer, using $\text{CuK}\alpha$ ($\lambda = 1.5406 \text{ \AA}$) radiation in a 2θ range of $5\text{--}50^\circ$.

FT-IR spectra were obtained on a Perkin-Elmer 65 IR spectrometer equipped with a Specac Quest ATR attenuated total reflection accessory in a wavenumber range of $400\text{--}4,000 \text{ cm}^{-1}$.

Thermal analysis (TGA/DTA) of the samples up to 900°C was carried out using a Jupiter NETZSCH STA 449 F1 instrument in air, with a heating rate of $10^\circ\text{C}/\text{min}$.

^{19}F NMR spectra of ionogels were recorded using a Bruker Avance II-300 spectrometer operating at 282.404 MHz and with inner stabilisation by deuterium. CCl_3F was used as a standard. For the measurements, ionogel samples were ground into coarse ($0.5\text{--}1 \text{ mm}$) powders and loaded in conventional (inner diam. 4.2 mm) NMR cuvettes for liquid samples, and measured using a liquid-state NMR detector.

Electron microscopy images were recorded on a Tescan Amber GMH scanning electron microscope (SEM) at 1 kV acceleration voltage. For the measurements, no conductive material was sputtered on the surface of the samples.

For some measurements (SEM, BJH), an ionic liquid was removed from an ionogel to obtain a bare silica porous solid. For this, ionogel samples were soaked in an excess of acetonitrile for a day, then the solvent was replaced by pure acetonitrile. This washing procedure was repeated three times. Finally, acetonitrile was removed by drying the samples in supercritical CO_2 (see above).

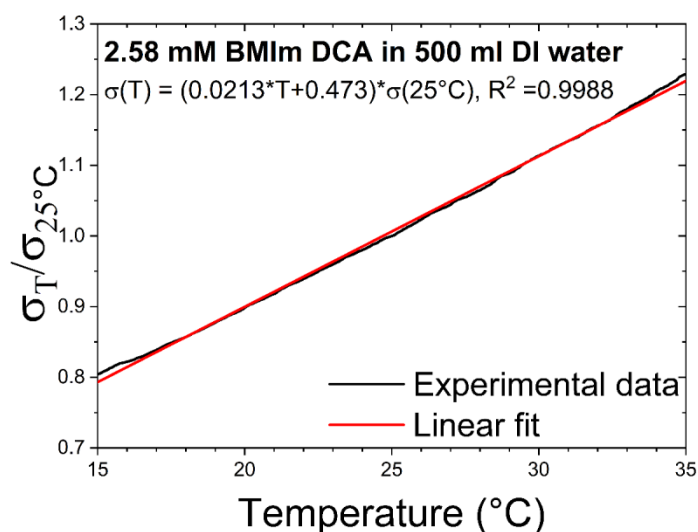


Figure S1. Temperature dependence of the conductivity of BMIm DCA water solution in the $15\text{--}35^\circ\text{C}$ temperature range.

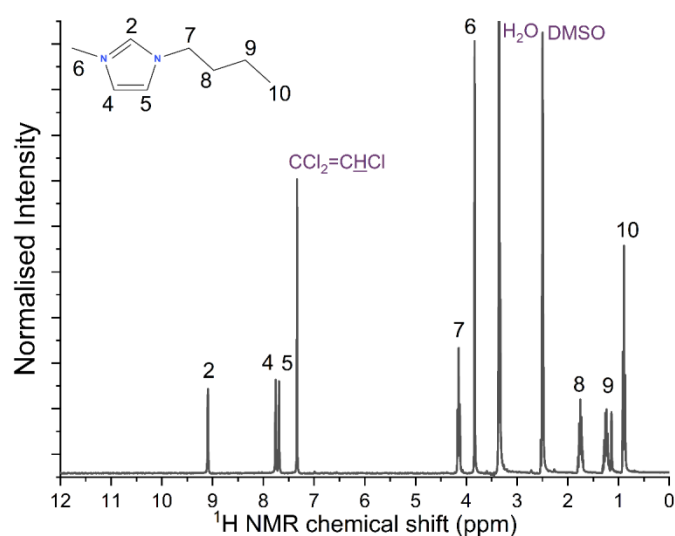


Figure S2. ^1H NMR spectrum of the liquid sample taken after 1h of the TMOS-C₄DCA washout experiment. BMIm signals were attributed according to [8].

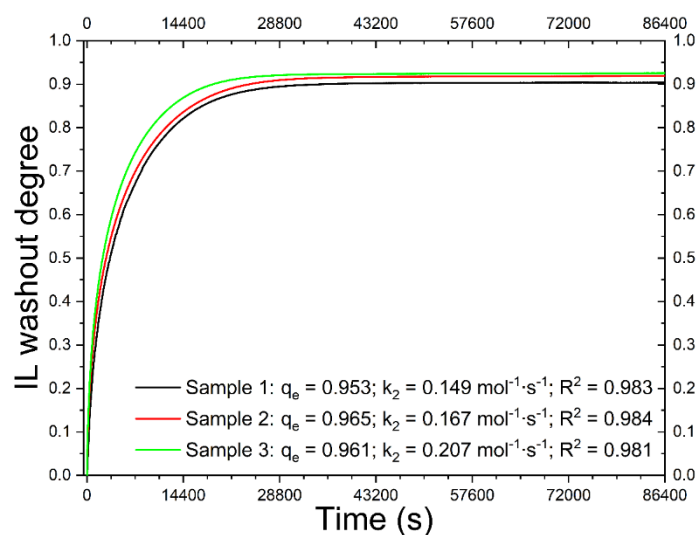


Figure S3. Reproducibility of washout kinetic curves: washout experiments for three TMOS-C₄DCA ionogels obtained from a single batch.

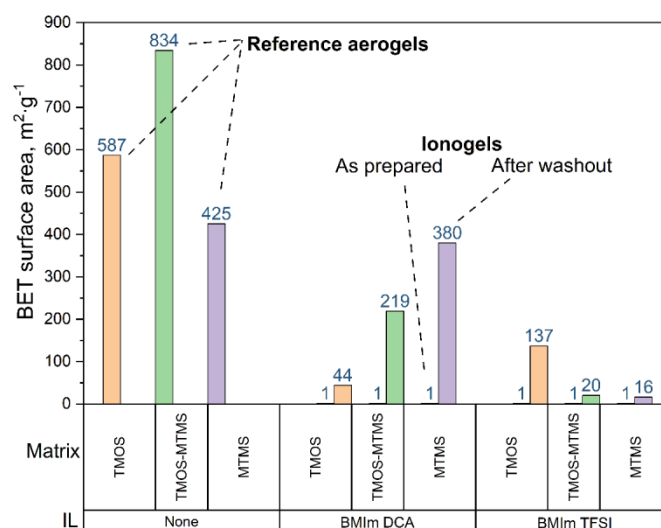


Figure S4. Specific surface area of the ionogels before and after the washout experiments.

Table S2. IR vibration bands attribution for reference silica aerogels.

Vibration Band Peak Position, cm ⁻¹			Vibration Band Attribution [9]
TMOS	TMOS-MTMS	MTMS	
438	434	422	$\delta(\text{O-Si-O})$
569	548	551	$\nu(\text{Si-O})$
-	741	762	$\rho(\text{CH}_2)$; surface methyl fragments
803	830	766	$\nu_s(\text{Si-O})$
-		840	$\nu(\text{Si-C})$; surface methyl fragments
948	932	905	$\nu_b(\text{Si-O})$
1060	1047	1015	$\nu_{as}(\text{Si-O-Si})$, TO mode
1138	1118	1102	$\nu_{as}(\text{Si-O-Si})$, LO mode
-	1275	1273	$\delta_s(\text{C-H})$, surface methyl fragments
1381	1313	1369	$\delta(-\text{CH}_2-)$
-	1415	1411	$\delta_{as}(\text{C-H})$, surface methyl fragments
1466	1461	-	$\delta(\text{C-H})$, methanol
1636	1620	-	$\delta(\text{H-O-H})$
-	2916	2918	$\nu_{as}(\text{CH}_3)$
2978	2978	2972	$\nu_s(\text{CH}_3)$
3300	-	-	O-H and SiO-H

Table S3. BMIm DCA ionogels and bare IL IR vibration bands attribution.

Vibration Band Peak Position, cm ⁻¹						Vibration Band Attribution	
TMOS-DCA		TMOS-MTMS-DCA		MTMS-DCA		BMIm DCA	
As Prepared	After Washout	As Prepared	After Washout	As Prepared	After Washout		
432	434	432	–	430	432	–	δ(O–Si–O) [9]
522	–	520	–	520	–	520	γ _s (N–C≡N) (A ₂) [10]
554	548	552	537	548	550	–	ν(Si–O) [9]
620	–	622	–	620	–	622	γ(N–Bu), ring puckering [11]
648	–	650	–	650	–	650	δ(C–N–C) [10]
696	–	704	–	694	678	696	ν(N–Me), ν(N–Bu) [11]
790	784	788	770	768	762	–	ν _s (Si–O) [9]
–	–	830	–	846	–	846	ρ(CH ₃ , CH ₂) [12]
913	–	915	–	912	–	900	ν _s (C–C–C), butyl [13]
964	946	942	–	934	918	–	ν _b (Si–O) [9]
964	–	952	–	–	–	948	ν _{as} (C–N), ν _{as} (C–C) [10]
1047	–	1036	1029	1018	–	1024	δ(H–C–C–H) + ρ(CH ₃) + ν(C–N) combination band [12]
1048	1058	1036	1032	1022	1005	–	ν _{as} (Si–O–Si), TO mode [9]
1135	1117	1083	1099	1110	1092	–	ν _{as} (Si–O–Si), LO mode [9]
1160	–	1161	–	1164	1166	1166	ρ(CH ₂) [12]
–	–	1274	1274	–	1270	–	δ _s (C–H), surface methyl fragments [9]
1316	–	1316	–	1313	–	1304	ν _{as} (N–C) [10]
1382	–	1384	–	1384	1378	1382	Imidazolium ring breathing [14]

–	–	–	1410	–	–	–	$\delta_{as}(\text{C-H})$, surface methyl fragments [9]
1428	–	1426	–	1426	–	1428	$\nu_{ring}, \delta(\text{CH}_2)$ [11]
1462	1466	1464	1460	1462	–	1460	$\rho(\text{CH}_3) + \nu(\text{CN})$ combination band [14]
1462	1466	1464	1460	1462	–	–	$\delta(\text{C-H})$, methanol [9]
1570	–	1570	–	1570	–	1568	$\nu(\text{CH}_2(\text{N}), \text{CH}_3(\text{N}))$ [14]
1626	1638	1640	1640	1640	1640	1624	$\delta(\text{H-O-H})$ [9]
2136	–	2134	–	2134	2148	2126	$\nu_{as}(\text{C}\equiv\text{N})$ (B_2) [10]
2200	–	2198	–	2198	–	2192	$\nu_s(\text{C}\equiv\text{N})$ (A_1) [10]
2238	–	2238	–	2238	–	2226	Femi enhanced $\nu_s(\text{N-C}) + \nu_{as}(\text{N-C})$ combination band [11]
2312	–	2316	–	2314	–	2310	Non attributed dicyanamide anion vibration
2876	2870	2874	2879	2874	2867	2872	$\nu_s(\text{CH}_2)$ [15]
2940	2930	2945	2923	2941	2924	2938	$\nu_{as}(\text{CH}_2)$ [15]
2962	–	2967	2965	2967	2971	2960	$\nu_s(\text{CH}_3)$ [15]
3034	–	3044	–	3030	–	3018	$\nu(\text{C}_2\text{-H})$, imidazolium ring [16]
3108	3081	3106	–	3105	–	3100	$\nu(\text{C}_4\text{-H}, \text{C}_5\text{-H})$ imidazolium ring [16]
3152	–	3175	–	3155	–	3146	$\nu_s(\text{CH}_2)$ [15]
3256,3402,3740	3344	3400,3455	3255,3448	3268,3383,3448,3742	3250,3446	3266,3428,3490	various SiO-H, HO-H and MeO-H stretching bands

Table S4. BMIm TFSI ionogels and bare IL IR vibration bands attribution.

Vibration Band Peak Position, cm^{-1}						Vibration Band Attribution	
TMOS-TFSI		TMOS-MTMS-TFSI		MTMS-TFSI		BMIm TFSI	
As Prepared	After Washout	As Prepared	After Washout	As Prepared	After Washout		
404	418	404	406	<400	<400	406	$\omega(\text{SO}_2)$ [10]
434	434	434	–	435	426	–	$\delta(\text{O-Si-O})$ [9]
508	–	508	508	510	510	509	Non-attributed TFSI vibration [10]
568	562	568	568	568	568	568	$\delta(\text{CF}_3)$ [10]
608	612	610	610	609	609	608	$\delta(\text{SO}_2)$ [10]
652	652	652	652	653	653	653	$\delta(\text{S-N-S})$ [10]
740	728	742	734	738	737	739	$\nu_s(\text{S-N-S})$ [10]
758	–	760	780	769	767	756	$\nu_s(\text{S-N-S})$ [10]
790	786	785	780	–	–	790	$\nu(\text{C-S})$ [10]
893	–	836	34	839	848	842	$\rho(\text{CH}_3, \text{CH}_2)$ [12]
–	–	918	929	910	916	–	$\nu_s(\text{C-C-C})$, butyl [13]
975	968	952	929	–	–	–	$\nu_b(\text{Si-O})$ [9]
1044	1058	1041	1027	1052	1055	1050	Non-attributed TFSI vibration [10]
1089	1058	1048	1027	1052	1055		$\nu_{as}(\text{Si-O-Si})$, TO mode [9]
1126	1124	1129	1104	1113	1107	–	$\nu_{as}(\text{Si-O-Si})$, LO mode [9]

1126	1124	1129	1124	1133	–	1134	$\nu_s(\text{SO}_2)$ [10]
1178	–	1183	1189	1186	1194	1176	$\delta(\text{H-C-C})$ and $\delta(\text{H-C-N})$ in imidazolium ring [15]
1228	–	1230	1230	1228	–	1211	Non-attributed TFSI vibration [10]
–	–	1273	1274	1272	1270	–	$\delta_s(\text{C-H})$, surface methyl fragments [9]
1339	1342	1331	1332	1340	1337	1340	$\nu_{as}(\text{SO}_2)$ [10]
1352	–	1351	1351	1351	1352	–	$\delta(-\text{CH}_2-)$ [9]
1465	1460	1465	1464	1459	1468	1464	$\rho(\text{CH}_3) + \nu(\text{CN})$ combination band [14]
1571	1578	1571	1576	1571	1574	1573	$\nu(\text{CH}_2(\text{N}), \text{CH}_3(\text{N}))$ [14]
1608	1634	–	1632	–	1636	–	$\delta(\text{H-O-H})$ [9]
2878	2875	2880	2878	2878	2882	2878	$\nu_s(\text{CH}_2)$ [15]
2958	2933	2920	2936	2956	2934	2939	$\nu_{as}(\text{CH}_2)$ [15]
2980	2960	2967	2966	2971	2970	2971	$\nu_s(\text{CH}_3)$ [15]
3138	–	3116	3110	3130	–	3114	$\nu(\text{C}_2\text{-H})$, imidazolium ring [16]
3162	3169	3165	3164	3164	3162	3162	$\nu(\text{C}_4\text{-H}, \text{C}_5\text{-H})$ imidazolium ring [16]
3494	3388	–	3388	3471	3400	3560	$\nu_{as}(\text{OH})$, free water [16]
–	–	~3600	–	–	3587	3643	$\nu_{as}(\text{OH})$, H-bonded water [16]

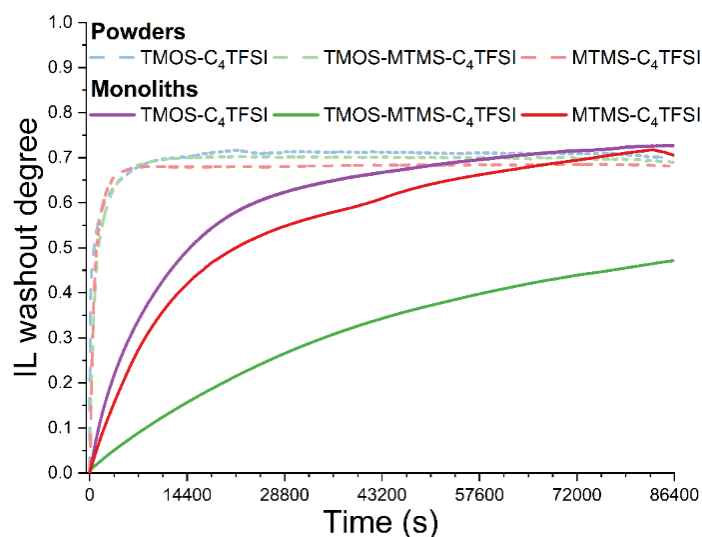


Figure S5. Washout kinetic curves for BMIIm TFSI ionogels in the form of a monolith and the corresponding powder.

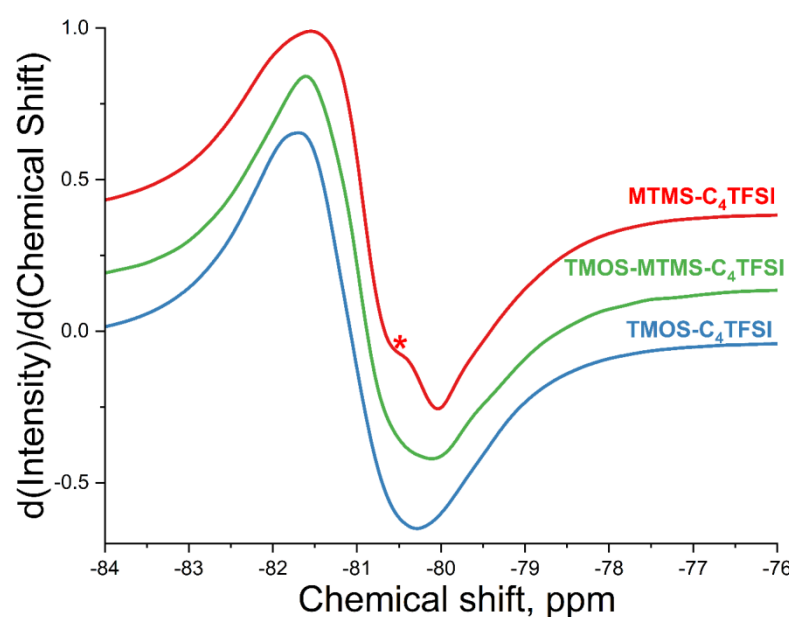


Figure S6. 1st order derivative of ^{19}F NMR intensity for BMIm TFSI ionogels, revealing two peak components for the MTMS- C_4TFSI sample.

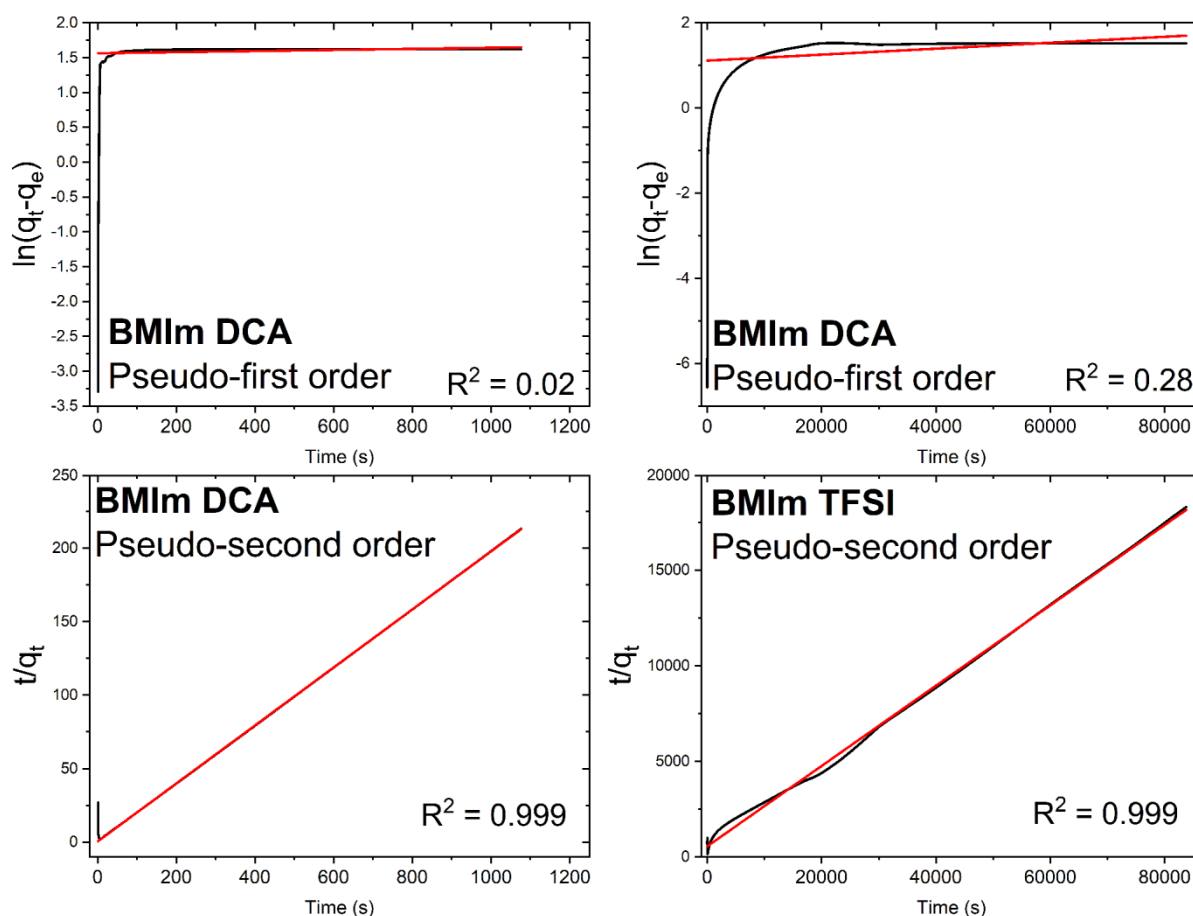


Figure S7. Kinetic curves for the dissolution of BMIm DCA and BMIm TFSI in water and their fitting to pseudo-1st and pseudo-2nd order kinetic models.

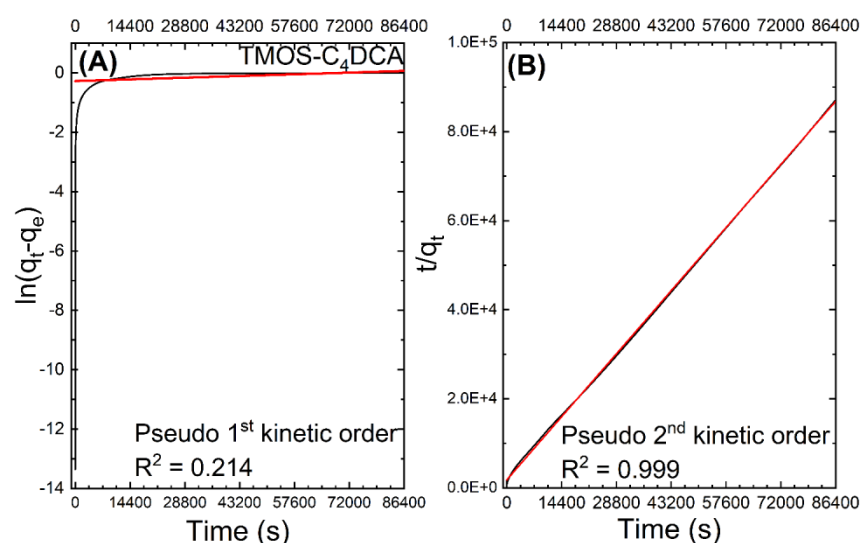


Figure S8. Comparison of pseudo-1st (1) and pseudo-2nd (b) order washout kinetic curves for TMOS-C₄DCA sample.

References

1. Zec, N.; Bešter-Rogač, M.; Marolt, G.; Vraneš, M.; Gadžurić, S. Electrical and Electrochemical Behavior of [Bmim][DCA] + γ -Butyrolactone Electrolyte. *J. Chem. Thermodyn.* **2016**, *101*, 293–299, doi:10.1016/j.jct.2016.06.017.
2. Waryo, T.T.; Qwasha, S.; Baker, P.G.; Iwuoha, E.I. Electrode Material Properties and Modelling of 1-Methyl-3-Octylimidazolium Bis(Trifluoromethylsulfonyl)Imide Ionic Liquid/ Paraffin Carbon Pastes. *Int. J. Electrochem. Sci.* **2016**, *11*, 4410–4426, doi:10.20964/2016.06.63.
3. Ranke, J.; Othman, A.; Fan, P.; Müller, A. Explaining Ionic Liquid Water Solubility in Terms of Cation and Anion Hydrophobicity. *Int. J. Mol. Sci.* **2009**, *10*, 1271–1289, doi:10.3390/ijms10031271.
4. Papaiconomou, N.; Yakelis, N.; Salminen, J.; Bergman, R.; Prausnitz, J.M. Synthesis and Properties of Seven Ionic Liquids Containing 1-Methyl-3-Octylimidazolium or 1-Butyl-4-Methylpyridinium Cations. *J. Chem. Eng. Data* **2006**, *51*, 1389–1393, doi:10.1021/je060096y.
5. Rouquerol, J.; Llewellyn, P.; Rouquerol, F. Is the Bet Equation Applicable to Microporous Adsorbents? *Stud. Surf. Sci. Catal.* **2007**, *160*, 49–56, doi:10.1016/S0167-2991(07)80008-5.
6. Thommes, M.; Kaneko, K.; Neimark, A. V.; Olivier, J.P.; Rodriguez-Reinoso, F.; Rouquerol, J.; Sing, K.S.W. Physisorption of Gases, with Special Reference to the Evaluation of Surface Area and Pore Size Distribution (IUPAC Technical Report). *Pure Appl. Chem.* **2015**, *87*, 1051–1069, doi:10.1515/pac-2014-1117.
7. Iacomì, P.; Llewellyn, P.L. PyGAPS: A Python-Based Framework for Adsorption Isotherm Processing and Material Characterisation. *Adsorption* **2019**, *25*, 1533–1542, doi:10.1007/s10450-019-00168-5.
8. Kaszyńska, J.; Rachocki, A.; Bielejewski, M.; Tritt-Goc, J. Influence of Cellulose Gel Matrix on BMIMCl Ionic Liquid Dynamics and Conductivity. *Cellulose* **2017**, *24*, 1641–1655, doi:10.1007/s10570-017-1223-z.
9. Al-Oweini, R.; El-Rassy, H. Synthesis and Characterization by FTIR Spectroscopy of Silica Aerogels Prepared Using Several Si(OR)₄ and R'Si(OR)₃ Precursors. *J. Mol. Struct.* **2009**, *919*, 140–145, doi:10.1016/j.molstruc.2008.08.025.
10. Paschoal, V.H.; Faria, L.F.O.; Ribeiro, M.C.C. Vibrational Spectroscopy of Ionic Liquids. *Chem. Rev.* **2017**, *117*, 7053–7112, doi:10.1021/acs.chemrev.6b00461.
11. Brotton, S.J.; Lucas, M.; Jensen, T.N.; Anderson, S.L.; Kaiser, R.I. Spectroscopic Study on the Intermediates and Reaction Rates in the Oxidation of Levitated Droplets of Energetic Ionic Liquids by Nitrogen Dioxide. *J. Phys. Chem. A* **2018**, *122*, 7351–7377, doi:10.1021/acs.jpca.8b05244.
12. Liu, J.; Zhou, W.; Chambreau, S.D.; Vaghjiani, G.L. Molecular Dynamics Simulations and Product Vibrational Spectral Analysis for the Reactions of NO₂ with 1-Ethyl-3-Methylimidazolium Dicyanamide (EMIM + DCA –), 1-Butyl-3-Methylimidazolium Dicyanamide (BMIM + DCA –), and 1-Allyl-3-Methylimidazolium Dicya. *J. Phys. Chem. B* **2020**, *124*, 4303–4325, doi:10.1021/acs.jpcc.0c02253.
13. Noack, K.; Schulz, P.S.; Paape, N.; Kiefer, J.; Wasserscheid, P.; Leipertz, A. The Role of the C2 Position in Interionic Interactions of Imidazolium Based Ionic Liquids: A Vibrational and NMR Spectroscopic Study. *Phys. Chem. Chem. Phys.* **2010**, *12*, 14153, doi:10.1039/c0cp00486c.
14. Grishina, E.P.; Ramenskaya, L.M.; Kudryakova, N.O.; Vagin, K.V.; Kraev, A.S.; Agafonov, A.V. Composite Nanomaterials Based on 1-Butyl-3-Methylimidazolium Dicyanamide and Clays. *J. Mater. Res. Technol.* **2019**, *8*, 4387–4398, doi:10.1016/j.jmrt.2019.07.050.

-
15. Elmahdy, M.M.; Fahmy, T.; Aldhafeeri, K.A.; Ibnouf, E.O.; Riadi, Y. Optical and Antibacterial Properties of 1-Butyl-3-Methylimidazolium Ionic Liquids with Trifluoromethanesulfonate or Tetrafluoroborate Anion. *Mater. Chem. Phys.* **2021**, *264*, 124369, doi:10.1016/j.matchemphys.2021.124369.
 16. Liu, Z.; El Abedin, S.Z.; Endres, F. Raman and FTIR Spectroscopic Studies of 1-Ethyl-3-methylimidazolium Trifluoromethylsulfonate, Its Mixtures with Water and the Solvation of Zinc Ions. *ChemPhysChem* **2015**, *16*, 970–977, doi:10.1002/cphc.201402831.